Published in final edited form as:
Neuroimage. 2010 November 1; 53(2): 471–479. doi:10.1016/j.neuroimage.2010.06.050.

Fractal Dimension Analysis of the Cortical Ribbon in Mild Alzheimer's Disease

Richard D. King[1], **Brandon Brown**[1], **Michael Hwang**[2], **Tina Jeon**[2], **Anuh T. George**[2], and **the Alzheimer's Disease Neuroimaging Initiative**[*]

[1] Department of Neurology, University of Utah

[2] Department of Neurology, University of Texas Southwestern Medical Center

Abstract

Fractal analysis methods are used to quantify the complexity of the human cerebral cortex. Many recent studies have focused on high resolution three-dimensional reconstructions of either the outer (pial) surface of the brain or the junction between the grey and white matter, but ignore the structure between these surfaces. This study uses a new method to incorporate the entire cortical thickness. Data were obtained from the Alzheimer's Disease (AD) Neuroimaging Initiative database (Control N=35, Mild AD N=35). Image segmentation was performed using a semi-automated analysis program. The fractal dimensions of three cortical models (the pial surface, grey/white surface and entire cortical ribbon) were calculated using a custom cube-counting triangle-intersection algorithm. The fractal dimension of the cortical ribbon showed highly significant differences between control and AD subjects (p<0.001). The inner surface analysis also found smaller but significant differences (p< 0.05). The pial surface dimensionality was not significantly different between the two groups. All three models had a significant positive correlation with the cortical gyrification index (r > 0.55, p<0.001). Only the cortical ribbon had a significant correlation with cortical thickness (r = 0.832, p< 0.001) and the Alzheimer's Disease Assessment Scale cognitive battery (r = −0.513, p = 0.002). The cortical ribbon dimensionality showed a larger effect size (d=1.12) in separating control and mild AD subjects than cortical thickness (d=1.01) or gyrification index (d=0.84). The methodological change shown in this paper may allow for further clinical application of cortical fractal dimension as a biomarker for structural changes that accrue with neurodegenerative diseases.

Keywords

Fractal Dimension; Cortex; Complexity; Alzheimer's disease; Cortical Thickness; Gyrification Index

Correspondence should be addressed to: Richard D. King, MD, PhD, Director, Alzheimer's Image Analysis Laboratory, Center for Alzheimer's Care, Imaging and Research, Department of Neurology, 650 Komas Dr. #106 A, Salt Lake City, UT 84104, Office: 801-585-6546, Fax: 801-581-2483, richard.king@hsc.utah.edu.

[*]Data used in the preparation of this article were obtained from the Alzheimer's Disease Neuroimaging Initiative (ADNI) database (www.loni.ucla.edu/ADNI). As such, the investigators within the ADNI contributed to the design and implementation of ADNI and/or provided data but did not participate in the analysis or writing of this report.

1. Introduction

Neuroimaging studies in recent years have highlighted the numerous important properties of the human cerebral cortex. One of the more interesting characteristics of the cortex is that it displays fractal properties (*i.e.* statistical similarity in shape) over a range of spatial scales (Bullmore et al., 1994; Free et al., 1996; Im et al., 2006; Jiang et al., 2008; Kiselev et al., 2003; Lee et al., 2004; Majumdar and Prasad, 1988). These fractal properties arise secondary to the folding of the cortex (Hofman, 1991). The complexity of the brain can be quantified by a numerical value known as fractal dimension (Mandelbrot, 1977, 1982). The underlying cerebral white matter, as well as the cerebellum and supporting white matter tracts are amenable to study using fractal approaches (Esteban et al., 2007; Liu et al., 2003; Wu et al., 2010; Zhang et al., 2006a; Zhang et al., 2006b). This approach has been used to study gender differences (Luders et al., 2004), epilepsy (Cook et al., 1995), schizophrenia (Casanova et al., 1989; Casanova et al., 1990; Ha et al., 2005; Narr et al., 2004; Sandu et al., 2008), stroke (Zhang et al., 2008), multiple sclerosis (Esteban et al., 2009), cortical development (Blanton et al., 2001; Thompson et al., 2005; Wu et al., 2009), cerebellar degeneration (Wu et al., 2010) and Alzheimer's disease (King et al., 2009).

There are many methods for computing the fractal dimension of the cerebral cortex. Initial studies used discontinuous voxel-based images as the basis for the fractal analysis. With the advancement of surface-based reconstructions over the past ten years, it is now possible to semi-automatically generate three-dimensional continuous tessellated polygon models of the inner and outer cortical surface. These surface reconstructions offer sub-millimeter resolution, and are ideal targets for shape analysis (Im et al., 2006; Jiang et al., 2008; Luders et al., 2004).

Two recent studies using three-dimensional cortical surface reconstructions have documented the correlation between fractal dimension and other features of shape including folding area, sulcal depth, cortical thickness, and curvature (Im et al., 2006; Jiang et al., 2008). These studies found a strong positive correlation with the folding measures, but a weak negative correlation with cortical thickness. In these studies, an infinitely thin surface model (the pial surface of the cortex) was used as the basis for the complexity measurement. The thickness of the cortex was not felt to have a significant influence on the fractal assessment of the cortical shape. However, other work using two-dimensional profiles of the cortical ribbon derived from the three-dimensional surface reconstructions demonstrated a strong positive correlation between fractal dimension and cortical thickness as well as gyrification index (King et al., 2009). Thus, neurodegenerative changes that decrease both cortical thickness and gyrification index have complementary effects. Methods that directly incorporate cortical thickness into the fractal complexity measure may be more sensitive for detecting shape changes that result from neurodegeneration.

The purpose of this paper is to describe a robust method for computing the fractal dimension of the cortical ribbon (*e.g.* the cortical surfaces and the structure between them). The fractal properties of the cortical ribbon will be compared with that of the pial surface as well as the surface reconstruction of the interface between the grey matter and the white matter (grey/white junction). We will compare the clinical utility of the cortical ribbon to the pial and grey/white surfaces in terms of capturing atrophic changes that occur with Alzheimer's disease. We then compare the cortical ribbon directly to cortical thickness and gyrification index measures. We hypothesize that fractal analysis of the cortical ribbon will be superior to analysis of either the pial or grey/white surfaces because these analyses will directly incorporate cortical thickness, which is known to be strongly affected by Alzheimer's disease. Furthermore, the fractal dimension of the cortical ribbon will have a greater distinction (as measured by effect

size) between normal controls and mild Alzheimer's disease patients compared to cortical thickness or gyrification index measures.

2. Methods and Materials

2.1 Source Data

The data used in this article were obtained from the Alzheimer's Disease Neuroimaging Initiative (ADNI) database (www.loni.ucla.edu/ADNI). The ADNI project was launched in 2003 by the National Institute on Aging (NIA), the National Institute of Biomedical Imaging and Bioengineering (NIBIB), the Food and Drug Administration (FDA), by private pharmaceutical companies, and by non-profit organizations, as a $60 million, 5-year public-private partnership. The primary goal of ADNI has been to test whether serial magnetic resonance imaging (MRI), positron emission tomography (PET), other biological markers, and clinical and neuropsychological assessment can be combined to measure the progression of mild cognitive impairment (MCI) and early Alzheimer's disease (AD). Anatomic data was obtained using the MP RAGE sequence (magnetization-prepared 180 degrees radio-frequency pulses and rapid gradient-echo). The parameters are: axial orientation, 6.4ms TR, 4.4ms TE, 12° FA, 49.9 kHz BW (195Hz/px), 24×19.2cm FOV, 256×192 matrix, 124 contiguous partitions, each 1.2 mm in thickness. The inversion time (TI) and the delay time (TD) are 1000ms and 500ms respectively. For up-to-date information see www.adni-info.org.

MP-RAGE Images from 70 patients (39 Male, 31 Female) were selected from the on-line database. There were 35 control subjects (75.0 ± 5.0 years old, Clinical Dementia Rating score = 0) and 35 subjects with mild Alzheimer's disease (75.4 ± 7.1 years old, Clinical Dementia Rating score = 1–2). The ages were not statistically different between groups ($p = 0.798$). Two patients in the mild Alzheimer's disease group were missing data from the ADAS-cog test at the time of data download.

2.2 Segmentation procedure

Images segmentation was performed using *FreeSurfer*. This semi-automated software suite has been described in detail in prior publications (Dale et al., 1999; Fischl et al., 2001; Fischl et al., 2002; Fischl et al., 1999; Fischl et al., 2004; Han et al., 2006; Jovicich et al., 2006; Segonne et al., 2007). Please refer to these publications for full details of the parameters used in the segmentation process. Briefly, processing the images occurred in several steps automatically through the *FreeSurfer* suite. The original images were converted from the DICOM format into a single file with all images from a particular scan protocol. Following motion correction and intensity normalization, extracerebral voxels were removed, using a "skull-stripping" procedure. Head position was normalized along the commissural axis, and then cortical regions were labeled using an automated procedure. A preliminary segmentation of the grey matter from the white matter was generated based on intensity differences and geometric structure differences in the grey/white junction (Fischl and Dale, 2000). The pial surface was generated using outward deformation of the grey/white surface with a second-order smoothness constraint (Dale et al., 1999; Fischl and Dale, 2000). The smoothness constraint allowed the pial surface to be extended into otherwise ambiguous areas. The resulting surfaces have sub-voxel accuracy. Examples of the 3D surface reconstruction of the pial and grey/white surfaces are shown in Figure 1. Cortical thickness measurements are generated during the segmentation and surface generation process. *FreeSurfer* was also used to calculate the gyrification index of each hemisphere.

2.3 Computing the Fractal Dimension of the Cortical Surfaces

The fractal dimension (f_{3D}) of the cortical surfaces was computed using a 3D cube-counting algorithm. This algorithm has been used by several previous investigators (Im et al., 2006;

Jiang et al., 2008), and has been found to be a robust and accurate method of computing cortical complexity (Jiang et al., 2008). The implementation of this algorithm is very similar to Jiang, et. al (2008). In brief, each 3D surface is composed of tessellated triangles (~200,000 per hemisphere). The intersection of each triangle (including the edges) with a cube matrix covering the entire brain is computed using standard geometry. Each cube is counted only once, resulting in a cube count of the total number of intersections. This process is shown in Figure 2. The cube size is then changed, and the intersection computation is repeated. f_{3D} is computed as the change in the log of the cube count divided by the change in the log of the cube size (see Equation 1).

$$f_{3D} = -\frac{\Delta \log(\text{cube count})}{\Delta \log(\text{cube size})} \quad (1)$$

Natural objects, such as the cerebral cortex, only possess fractal properties over a limited spatial scale. The range over which the fractal analysis is valid can be determined by measuring the consistency (scale invariance) in the cube count/size slope (Zhang et al., 2006b). Using a point-to-point slope cutoff of 0.1, the minimum spatial scale for all three cortical models (cortical ribbon, pial surface, and grey/white surface) was 0.5 mm. The upper range for all three cortical models was set to 15 mm, as this was the value identified in the vast majority of subjects. There was no difference in the spatial ranges determined for the three cortical models. Although still highly linear, both the pial surface and grey/white surface were less stable in terms of point-to-point slope compared to the cortical ribbon. The coefficient of determination (R^2) for the resulting regression lines were as follows: cortical ribbon > 0.9999, pial surface > 0.9984, grey/white surface > 0.9979. Please see King et al. (2009) for a graphical representation of this process.

This algorithm was implemented using a custom build software program called the *Cortical Complexity Calculator* (*C3*). *C3* was written on Mac OS X (10.5) using the XCode environment in Objective C with graphic implementation using OpenGL. The software directly reads the *FreeSurfer* surface files and performs the cube counting and regression calculations from native-space image data.

2.4 Analyzing the Cortical Ribbon by Generating Intermediate Surfaces

While the inner and outer cortical surfaces are represented by physical models, there is no actual model of the space between these surfaces generated by *FreeSurfer*. Without an extra step, many cubes between the surfaces would go uncounted. The number of intersecting cubes contained between the pial and grey/white surfaces increases exponentially as the cube size decreases. While it is possible to compute these intersections using vectors normal to each surface, there is no way to assure every box is counted. Instead, we solve this intersection problem by generating dynamic intermediate surfaces. We take advantage of the fact that the pial surface is itself a derivative of the initial grey/white segmentation. There is an exact 1:1 correspondence of vertices between these two surfaces. Note that the distance between the two surfaces is not uniform, but is in fact determined by the cortical thickness. The cortical thickness can range from 0 (in non-cortical sections of the surface, such as arbitrary triangles generated in the midline; these triangles are removed prior to fractal analysis) to a maximum thickness ~5 mm.

An intermediate surface can be generated by moving each vertex of grey/white surface a predetermined percent distance along a vector between the corresponding vertices of the pial and grey/white surfaces. In regions of higher cortical thickness, this distance is larger than in thinner regions. The number of surfaces needed to assure that no fractal counting cubes are

missed can be computed exactly as the maximum cortical thickness divided by the cube size. The intersection of these intermediate surfaces and the counting cubes can be computed using the same algorithm with the pial and grey/white surfaces. See Figure 3 for a graphic representation of this process.

2.5 Statistical Analysis

Group differences were computed using 2 sided t-tests and effect sizes were computed using Cohen's d statistic. Regression coefficients were computed using the least squares method. All analyses were performed using statistical functions within Microsoft Excel 2008 for Mac Version 12.2.4.

2.6 Approach

In this study, the f_{3D} of the pial surface, grey/white surface, and cortical ribbon were calculated, and the ability to distinguish control subjects from those with AD were computed. The three cortical models were then regressed against the cortical thickness, gyrification index, and ADAS-cog scores. The cortical thickness values and gyrification index values were also regressed against the ADAS-cog scores as well as each other. Finally, the ability of the cortical ribbon to distinguish control subjects from mild AD was compared to cortical thickness and gyrification index measures.

3. Results

3.1 Comparing the three cortical models

There was no significant difference between the cortical f_{3D} of men and women in either the control group ($p = 0.56$) or the mild Alzheimer's disease group ($p = 0.72$), although the women trended slightly higher on average. Comparison of the f_{3D} for control and AD subjects using the three cortical models are shown in Figure 4. For the pial surface, there was no significant difference between the f_{3D} of control subjects and those with Alzheimer's disease ($p = 0.27$, effect size $d = 0.26$). Fractal analysis of the grey/white junction did show a group difference that reached statistical significance ($p < 0.05$, effect size $d = 0.53$). When the cortical ribbon was used as the basis for the f_{3D} calculation, the group differences are highly significant ($p < 0.001$, effect size $d = 1.12$).

For comparison to previous studies (Im et al., 2006; Jiang et al., 2008), the correlation between f_{3D} and both cortical thickness and gyrification index (a measure of cortical folding) are shown in Figure 5A–B. As in the previous studies, the pial surface f_{3D} showed a strong positive correlation with gyrification index ($r = 0.679$, $p < 0.001$) and essentially no correlation with cortical thickness ($r = -0.024$, $p = 0.844$). The f_{3D} of the grey/white surface, which was not assessed in the previous papers referenced above, showed a strong positive correlation with gyrification index ($r = 0.586$, $p < 0.001$) and a weak negative correlation with cortical thickness ($r = -0.169$, $p = 0.168$). The f_{3D} of the cortical ribbon had a significant positive correlation with both gyrification index ($r = 0.555$, $p < 0.001$) and cortical thickness ($r = 0.832$, $p < 0.001$). Cortical thickness and gyrification index are poorly correlated with each other ($r = 0.184$, $p = 0.128$, data not shown).

In Figure 5C, the correlation between cortical f_{3D} and the Alzheimer's Disease Assessment Scale-Cognitive (ADAS-cog) is shown. The ADAS-cog is the most commonly used neuropsychiatric assessment battery in clinical trials in Alzheimer's disease. The f_{3D} of neither the pial surface ($r = -0.185$, $p = 0.286$) nor the grey/white surface ($r = -0.284$, $p = 0.098$) were significantly correlated to the ADAS-cog. The f_{3D} of the cortical ribbon did show a significant correlation with the ADAS-cog ($r = -0.513$, $p = 0.002$)

3.2 Comparing the cortical ribbon to cortical thickness and gyrification index

There is a statistically significant difference in the value of both cortical thickness ($p < 0.001$, d = 1.01) and gyrification index ($p < 0.001$, d = 0.84) between the control group and the mild AD group (see Figure 6). Note that the effect sizes are smaller than for the cortical ribbon f_{3D} ($p < 0.001$, effect size $d = 1.12$). Just like the cortical ribbon f_{3D} (r = −0.513, $p = 0.002$), the values of cortical thickness (r = −0.441, $p = 0.008$) and gyrification index (r = −0.418, $p = 0.012$) are negatively correlated with performance on the ADAS-cog (see Figure 7). ROC curves for all the measures used in this paper are shown in Figure 8. The area-under-the-curve values are as follows: cortical ribbon f_{3D} 0.837, pial surface f_{3D} 0.572, grey/white surface f_{3D} 0.671, Cortical thickness 0.798, and Gyrification index 0.734.

4. Discussion

While all three cortical models have a significant correlation with cortical folding (as measured by gyrification index), only the cortical ribbon has a strong correlation with cortical thickness measurements. Hence, known changes that occur in cortical thickness in Alzheimer's disease would be missed by the pial and grey/white cortical models. This likely accounts for much of the improved ability to discriminate between clinical groups used in this paper. It also may explain why the cortical ribbon was the only model to have a significant correlation with the ADAS-cog. All three cortical measures we have analyzed (cortical thickness, gyrification index and FD of the cortical ribbon) provided a significant difference between normal subjects and patients, even though the greatest effect size was obtained using the FD of the cortical ribbon. In terms of separating controls from mild AD patients, the area under the ROC curve analysis suggests that cortical ribbon f_{3D} is a "good" test, cortical thickness and gyrification index are "fair" tests, grey/white surface f_{3D} is a "poor" test, and pial surface f_{3D} is a "worthless" test.

Atrophic changes that occur on the pial surface could either increase or decrease the complexity, depending on how the atrophy occurs. For example, a change in the pial surface that decreased the folding area would decrease complexity; conversely, if the change increased sulcal depth, then the complexity would increase. Both types of changes are noted on the brains used in this study. By using the cortical ribbon, the conflicting effects on the pial surface are overcome by adding the complementary effects of the cortical thickness changes while also incorporating the structural changes occurring at the grey/white junction.

Our results also corroborated the well established observation that there are significant differences in the average cortical thickness of control subjects compared to patients with mild Alzheimer's disease. We also found that the gyrification index is also significantly different between control and mild AD patients. To the best of our knowledge, this effect has not been clearly documented in Alzheimer's disease.

The effect size using the cortical ribbon f_{3D} was larger than either using cortical thickness or using the gyrification index. Moreover, the fractal analysis technique using the cortical ribbon is able to account for more of the variance in the ADAS-cog scores than either the cortical thickness or gyrification index measures. This improved discrimination will likely be needed to correctly categorize less clinically distinct cases (*i.e.* normal vs. mild cognitive impairment).

There are many other structural factors that likely influence the cortical ribbon f_{3D}. Atrophic changes that occur at the grey/white junction are likely to be affected by volume change occurring in the sub-cortical white matter, basal ganglia, and lateral ventricles. These changes could be an important source of cortical fractal dimensionality change, and thus should not be removed in the context of this paper (*e.g.* transforming images into a Talairach space, covariance). Further exploration of the specific effects of changes in these volumetric factors,

along with other measures including normalized brain volume, age, or normalized cortical surface area, on cortical f_{3D} is needed.

The methods used in this paper take advantage of high-contrast magnetic resonance imaging to generate high-resolution three-dimensional continuous models of the cerebral cortex. This approach has been used in several other recent studies of high resolution models of the pial surface (Blanton et al., 2001; Im et al., 2006; Jiang et al., 2008; Luders et al., 2004; Narr et al., 2004; Sandu et al., 2008; Thompson et al., 2005) and grey/white junction surfaces (Sandu et al., 2008). These surface based methods provide higher resolution data than voxel-based masking methods. Consequently, using intermediate surfaces to generate fractal data from the entire cortical ribbon generates a continuous 3D volume model that is more topologically accurate than a grey matter voxel mask. Note that this limitation in using the grey matter voxel-mask may eventually be overcome using very high field (*i.e.* > 7 Tesla) high resolution images.

While this whole-brain fractal measure is quite promising, there are several limitations to this analysis technique. First, the whole-brain approach is generating an aggregate measure across the entire cerebral cortex. However, the atrophic changes that occur in Alzheimer's disease do not occur in all regions of the brain equally. There are also significant regional variations in cortical f_{3D} values (Jiang et al., 2008; King et al., 2009). This technique could be improved by performing a more localized analysis. This would be beneficial for several reasons. By focusing on regions of interest, the discriminative power could be significantly increased. Furthermore, different neurodegenerative diseases, such as Frontotemporal dementia and Dementia with Lewy Bodies, have very different asymmetric patterns of cortical involvement. Obtaining statistically normalized spatial maps will likely be needed to perform a prospective categorization. Moreover, the significant global atrophic changes associated with normal aging are not accounted for. In this paper, age was averaged within the two groups. A better method may utilize regression models to generate a map showing Z-scaled significant deviations comparing subjects to age-matched controls. These two methodological improvements are likely to greatly increase the sensitivity and specificity of the fractal analysis technique.

Finally, it is likely that no single imaging biomarker will have enough specificity and sensitivity for prospective diagnosis. Therefore, having as many complementary biomarkers as possible will aid in prospective categorization. Cortical f_{3D} could serve as an important adjunct to currently used imaging markers such as volumetric assessments (*i.e.* hippocampal volume, lateral ventricle volume), functional measures (*i.e.* Fluoro-deoxyglucose Positron emission tomography, functional magnetic resonance imaging), and direct amyloid binding agents (*i.e.* Pittsburg Compound B, AV45).

5. Conclusion

This study demonstrates the potential of using the f_{3D} of the cerebral cortical ribbon as a quantitative marker of cerebral cortex structure in mild Alzheimer's disease. The results of this paper suggest that studies of cerebral cortex f_{3D} may benefit from adapting their techniques to include analysis of the entire cortical ribbon. It is our hope that with continued development, fractal analysis methods will find a place alongside currently used morphometric and functional measures to help us provide better care for our patients suffering with neurodegenerative diseases.

Acknowledgments

The authors would like to thank Dr. Norman Foster, Dr. Denise Park and Dr. Roger Rosenberg for their unwavering support of this work. We would also like to thank Jeanette Berberich, True Price, Tyler Adams, Daniel Esponda, Kyle Nilson, Laura Yuan, Rigoberto Hernandez, Dr. Angela Wang, Dr. Thomas Fletcher, Dr. Kristen Kennedy, and Dr. Karen Rodrigue for their assistance on this project.

This paper was supported by the Center for Alzheimer's Care Imaging and Research at the University of Utah, and grants from the Robert Wood Johnson Foundation, National Institute of Aging (5-R37-AG006265-27 and 5-P30-AG012300-15), and the Alzheimer's Association. Data collection and sharing for this project was funded by the Alzheimer's Disease Neuroimaging Initiative (ADNI) (National Institutes of Health Grant U01 AG024904). ADNI is funded by the National Institute on Aging, the National Institute of Biomedical Imaging and Bioengineering, and through generous contributions from the following: Abbott, AstraZeneca AB, Bayer Schering Pharma AG, Bristol-Myers Squibb, Eisai Global Clinical Development, Elan Corporation, Genentech, GE Healthcare, GlaxoSmithKline, Innogenetics, Johnson and Johnson, Eli Lilly and Co., Medpace, Inc., Merck and Co., Inc., Novartis AG, Pfizer Inc, F. Hoffman-La Roche, Schering-Plough, Synarc, Inc., as well as non-profit partners the Alzheimer's Association and Alzheimer's Drug Discovery Foundation, with participation from the U.S. Food and Drug Administration. Private sector contributions to ADNI are facilitated by the Foundation for the National Institutes of Health (www.fnih.org <http://www.fnih.org/>). The grantee organization is the Northern California Institute for Research and Education, and the study is coordinated by the Alzheimer's Disease Cooperative Study at the University of California, San Diego. ADNI data are disseminated by the Laboratory for Neuro Imaging at the University of California, Los Angeles. This research was also supported by NIH grants P30 AG010129, K01 AG030514, and the Dana Foundation.

References Cited

Blanton RE, Levitt JG, Thompson PM, Narr KL, Capetillo-Cunliffe L, Nobel A, Singerman JD, McCracken JT, Toga AW. Mapping cortical asymmetry and complexity patterns in normal children. Psychiatry Res 2001;107:29–43. [PubMed: 11472862]

Bullmore E, Brammer M, Harvey I, Persaud R, Murray R, Ron M. Fractal analysis of the boundary between white matter and cerebral cortex in magnetic resonance images: a controlled study of schizophrenic and manic-depressive patients. Psychol Med 1994;24:771–781. [PubMed: 7991759]

Casanova MF, Daniel DG, Goldberg TE, Suddath RL, Weinberger DR. Shape analysis of the middle cranial fossa of schizophrenic patients. A computerized tomographic study. Schizophr Res 1989;2:333–338. [PubMed: 2487174]

Casanova MF, Goldberg TE, Suddath RL, Daniel DG, Rawlings R, Lloyd DG, Loats HL, Kleinman JE, Weinberger DR. Quantitative shape analysis of the temporal and prefrontal lobes of schizophrenic patients: a magnetic resonance image study. J Neuropsychiatry Clin Neurosci 1990;2:363–372. [PubMed: 2136388]

Cook MJ, Free SL, Manford MR, Fish DR, Shorvon SD, Stevens JM. Fractal description of cerebral cortical patterns in frontal lobe epilepsy. Eur Neurol 1995;35:327–335. [PubMed: 8591799]

Dale AM, Fischl B, Sereno MI. Cortical surface-based analysis. I. Segmentation and surface reconstruction. Neuroimage 1999;9:179–194. [PubMed: 9931268]

Esteban FJ, Sepulcre J, de Mendizabal NV, Goni J, Navas J, de Miras JR, Bejarano B, Masdeu JC, Villoslada P. Fractal dimension and white matter changes in multiple sclerosis. Neuroimage 2007;36:543–549. [PubMed: 17499522]

Esteban FJ, Sepulcre J, de Miras JR, Navas J, de Mendizabal NV, Goni J, Quesada JM, Bejarano B, Villoslada P. Fractal dimension analysis of grey matter in multiple sclerosis. J Neurol Sci 2009;282:67–71. [PubMed: 19167728]

Fischl B, Dale AM. Measuring the thickness of the human cerebral cortex from magnetic resonance images. Proc Natl Acad Sci U S A 2000;97:11050–11055. [PubMed: 10984517]

Fischl B, Liu A, Dale AM. Automated manifold surgery: constructing geometrically accurate and topologically correct models of the human cerebral cortex. IEEE Trans Med Imaging 2001;20:70–80. [PubMed: 11293693]

Fischl B, Salat DH, Busa E, Albert M, Dieterich M, Haselgrove C, van der Kouwe A, Killiany R, Kennedy D, Klaveness S, Montillo A, Makris N, Rosen B, Dale AM. Whole brain segmentation: automated labeling of neuroanatomical structures in the human brain. Neuron 2002;33:341–355. [PubMed: 11832223]

Fischl B, Sereno MI, Dale AM. Cortical surface-based analysis. II: Inflation, flattening, and a surface-based coordinate system. Neuroimage 1999;9:195–207. [PubMed: 9931269]

Fischl B, van der Kouwe A, Destrieux C, Halgren E, Segonne F, Salat DH, Busa E, Seidman LJ, Goldstein J, Kennedy D, Caviness V, Makris N, Rosen B, Dale AM. Automatically parcellating the human cerebral cortex. Cereb Cortex 2004;14:11–22. [PubMed: 14654453]

Free SL, Sisodiya SM, Cook MJ, Fish DR, Shorvon SD. Three-dimensional fractal analysis of the white matter surface from magnetic resonance images of the human brain. Cereb Cortex 1996;6:830–836. [PubMed: 8922340]

Ha TH, Yoon U, Lee KJ, Shin YW, Lee JM, Kim IY, Ha KS, Kim SI, Kwon JS. Fractal dimension of cerebral cortical surface in schizophrenia and obsessive-compulsive disorder. Neurosci Lett 2005;384:172–176. [PubMed: 15893428]

Han X, Jovicich J, Salat D, van der Kouwe A, Quinn B, Czanner S, Busa E, Pacheco J, Albert M, Killiany R, Maguire P, Rosas D, Makris N, Dale A, Dickerson B, Fischl B. Reliability of MRI-derived measurements of human cerebral cortical thickness: the effects of field strength, scanner upgrade and manufacturer. Neuroimage 2006;32:180–194. [PubMed: 16651008]

Hofman MA. The fractal geometry of convoluted brains. J Hirnforsch 1991;32:103–111. [PubMed: 1811015]

Im K, Lee JM, Yoon U, Shin YW, Hong SB, Kim IY, Kwon JS, Kim SI. Fractal dimension in human cortical surface: multiple regression analysis with cortical thickness, sulcal depth, and folding area. Hum Brain Mapp 2006;27:994–1003. [PubMed: 16671080]

Jiang J, Zhu W, Shi F, Zhang Y, Lin L, Jiang T. A robust and accurate algorithm for estimating the complexity of the cortical surface. J Neurosci Methods 2008;172:122–130. [PubMed: 18511127]

Jovicich J, Czanner S, Greve D, Haley E, van der Kouwe A, Gollub R, Kennedy D, Schmitt F, Brown G, Macfall J, Fischl B, Dale A. Reliability in multi-site structural MRI studies: effects of gradient non-linearity correction on phantom and human data. Neuroimage 2006;30:436–443. [PubMed: 16300968]

King RD, George AT, Jeon T, Hynan LS, Youn TS, Kennedy DN, Dickerson B. the Alzheimer's Disease Neuroimaging, I. Characterization of Atrophic Changes in the Cerebral Cortex Using Fractal Dimensional Analysis. Brain Imaging Behav 2009;3:154–166. [PubMed: 20740072]

Kiselev VG, Hahn KR, Auer DP. Is the brain cortex a fractal? Neuroimage 2003;20:1765–1774. [PubMed: 14642486]

Lee JM, Yoon U, Kim JJ, Kim IY, Lee DS, Kwon JS, Kim SI. Analysis of the hemispheric asymmetry using fractal dimension of a skeletonized cerebral surface. IEEE Trans Biomed Eng 2004;51:1494–1498. [PubMed: 15311838]

Liu JZ, Zhang LD, Yue GH. Fractal dimension in human cerebellum measured by magnetic resonance imaging. Biophys J 2003;85:4041–4046. [PubMed: 14645092]

Luders E, Narr KL, Thompson PM, Rex DE, Jancke L, Steinmetz H, Toga AW. Gender differences in cortical complexity. Nat Neurosci 2004;7:799–800. [PubMed: 15338563]

Majumdar S, Prasad RR. The fractal dimension of cerebral surfaces using magnetic resonance imaging. Computers in Physics 1988;2:69–73.

Mandelbrot, BB. Fractals: form, chance, and dimension. W. H. Freeman; San Francisco: 1977.

Mandelbrot, BB. The fractal geometry of nature. W.H. Freeman; San Francisco: 1982.

Narr KL, Bilder RM, Kim S, Thompson PM, Szeszko P, Robinson D, Luders E, Toga AW. Abnormal gyral complexity in first-episode schizophrenia. Biol Psychiatry 2004;55:859–867. [PubMed: 15050868]

Rosset A, Spadola L, Ratib O. OsiriX: an open-source software for navigating in multidimensional DICOM images. J Digit Imaging 2004;17:205–216. [PubMed: 15534753]

Sandu AL, Rasmussen IA Jr, Lundervold A, Kreuder F, Neckelmann G, Hugdahl K, Specht K. Fractal dimension analysis of MR images reveals grey matter structure irregularities in schizophrenia. Comput Med Imaging Graph 2008;32:150–158. [PubMed: 18068333]

Segonne F, Pacheco J, Fischl B. Geometrically accurate topology-correction of cortical surfaces using nonseparating loops. IEEE Trans Med Imaging 2007;26:518–529. [PubMed: 17427739]

Thompson PM, Lee AD, Dutton RA, Geaga JA, Hayashi KM, Eckert MA, Bellugi U, Galaburda AM, Korenberg JR, Mills DL, Toga AW, Reiss AL. Abnormal cortical complexity and thickness profiles mapped in Williams syndrome. J Neurosci 2005;25:4146–4158. [PubMed: 15843618]

Wu YT, Shyu KK, Chen TR, Guo WY. Using three-dimensional fractal dimension to analyze the complexity of fetal cortical surface from magnetic resonance images. Nonlinear Dynamics 2009;58:745–752.

Wu YT, Shyu KK, Jao CW, Wang ZY, Soong BW, Wu HM, Wang PS. Fractal dimension analysis for quantifying cerebellar morphological change of multiple system atrophy of the cerebellar type (MSA-C). Neuroimage 2010;49:539–551. [PubMed: 19635573]

Zhang L, Butler AJ, Sun CK, Sahgal V, Wittenberg GF, Yue GH. Fractal dimension assessment of brain white matter structural complexity post stroke in relation to upper-extremity motor function. Brain Res 2008;1228:229–240. [PubMed: 18590710]

Zhang L, Dean D, Liu JZ, Sahgal V, Wang X, Yue GH. Quantifying degeneration of white matter in normal aging using fractal dimension. Neurobiol Aging. 2006a

Zhang L, Liu JZ, Dean D, Sahgal V, Yue GH. A three-dimensional fractal analysis method for quantifying white matter structure in human brain. J Neurosci Methods 2006b;150:242–253. [PubMed: 16112737]

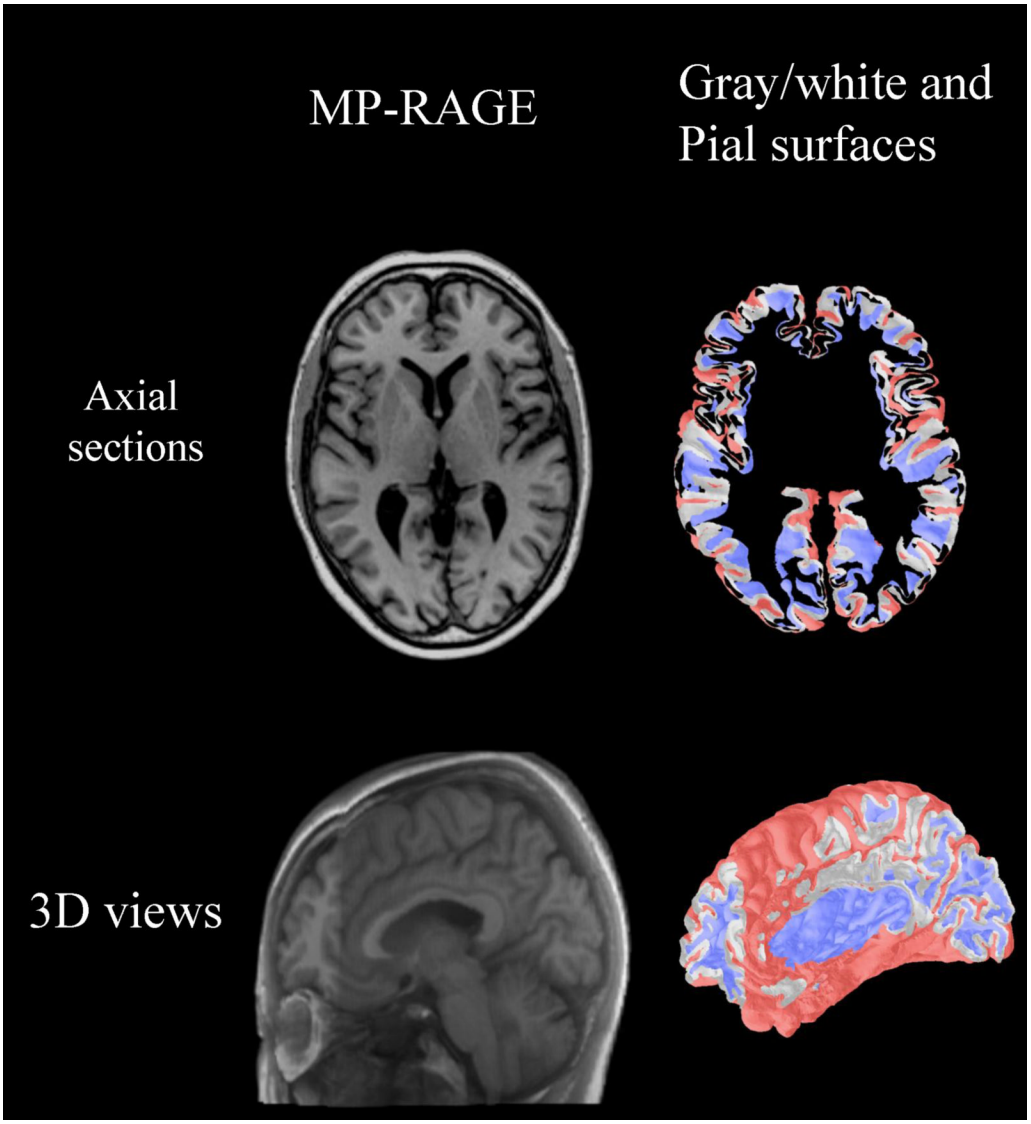

Figure 1. Example source data and resulting 3D surface models

(Left column) MP-RAGE image from a control subject in the ADNI database. The upper image is an axial section through the mid-thalamus. The lower panel shows a 3D reconstruction of the MP-RAGE generated using the Osirix 3D viewer (Rosset et al., 2004). **(Right Column)** The corresponding 3D surface models are shown. The outer edge of the pial surface is colored red, and the inside edge of the grey/white surface is colored blue. The edges between the pial and grey/white surface are both shown in grey. The slab shown in the upper panel is ~5mm thick. The ribbon appears wavy because the cortex has a high degree of curvature. The lower panel shows an oblique slice of both 3D surface models.

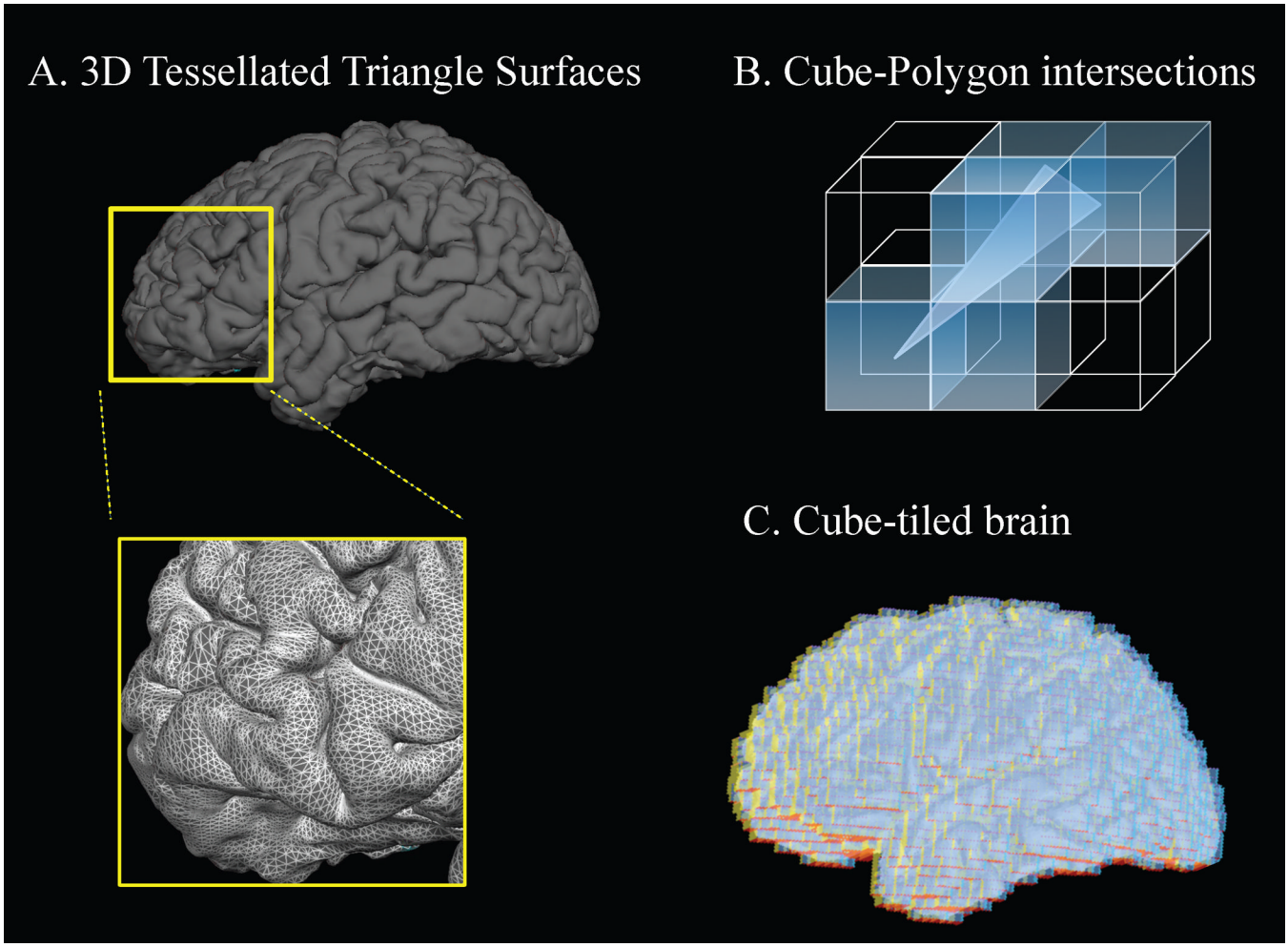

Figure 2. 3D cube/surface intersections

A. The upper panel shows the left hemisphere pial surface from a healthy control subject. A section is magnified with the triangular mesh displayed. **B.** Example of the intersection of a triangle with a lattice of cubes. Intersections are computed for each side of the triangle (which will count cubes that intersect either a side or a vertex). **C.** An example tiling of cubes over the pial surface.

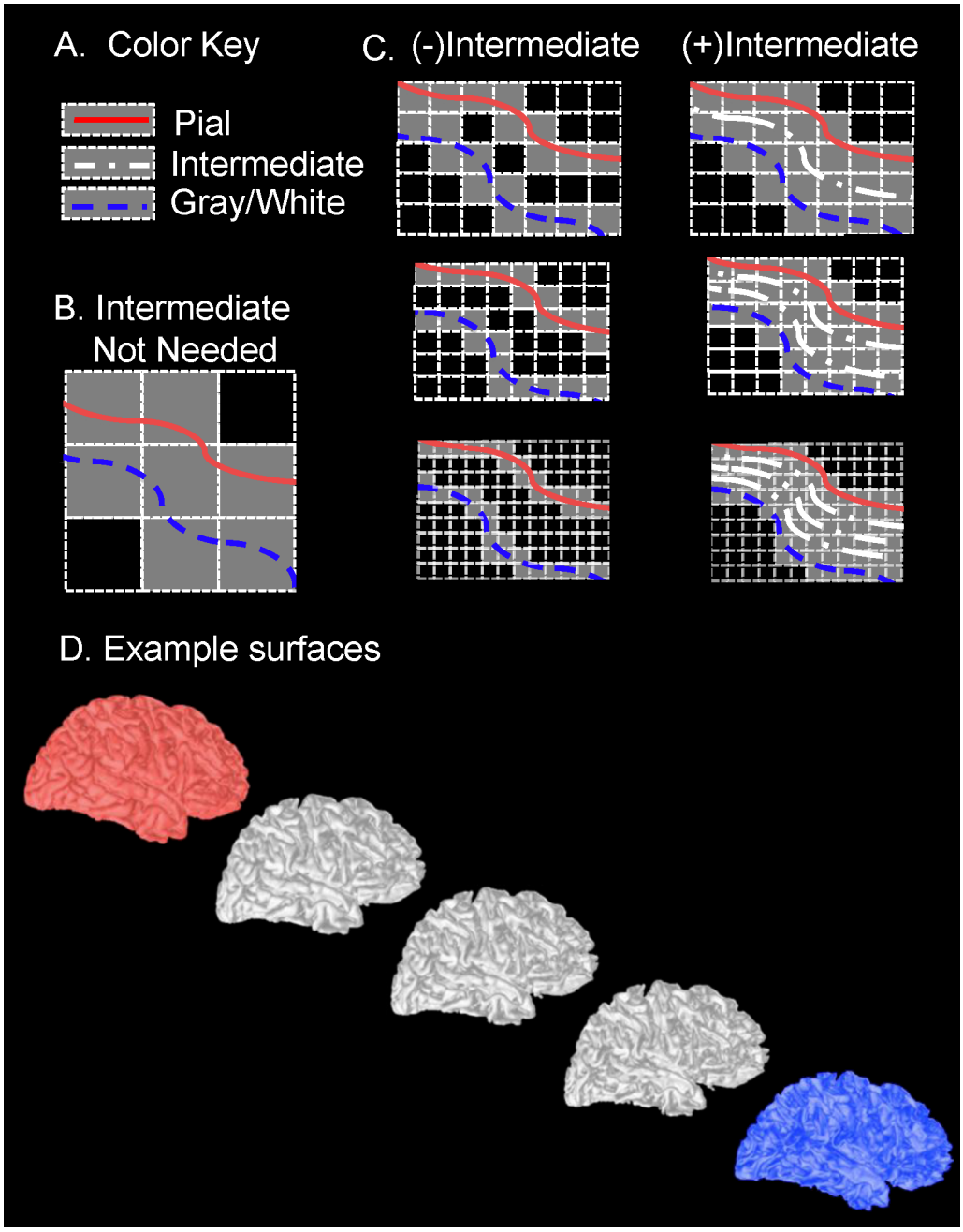

Figure 3. Intermediate surfaces capture cubes between the pial and grey/white surfaces

A–C. Simplified 2D projections are shown for the pial (red solid line), grey/white (blue dashed line) and intermediate (dash-dot line) surfaces. The cubes that intersect the surfaces are filled in grey, while non-intersecting cubes are left unfilled. **B**. When the cubes are large, no intermediate surfaces are needed. **C**. As the cube size decreases, more intermediate surfaces are needed to capture all the cubes located between the pial and grey/white surfaces. The left column shows the cube-cortex intersections without the intermediate surface, while the right column shows the intersections with intermediate surfaces. **D.** Intermediate surfaces can be generated dynamically as needed. Each point in the intermediate surface lies on a vector between corresponding vertices in the pial and grey/white surfaces. The percent distance along the vector determines the image. The pial surface is shown in red, and the grey/white surface

is blue. The grey surfaces represent intermediate surfaces 25%, 50%, and 75% of the way between the bounding surfaces.

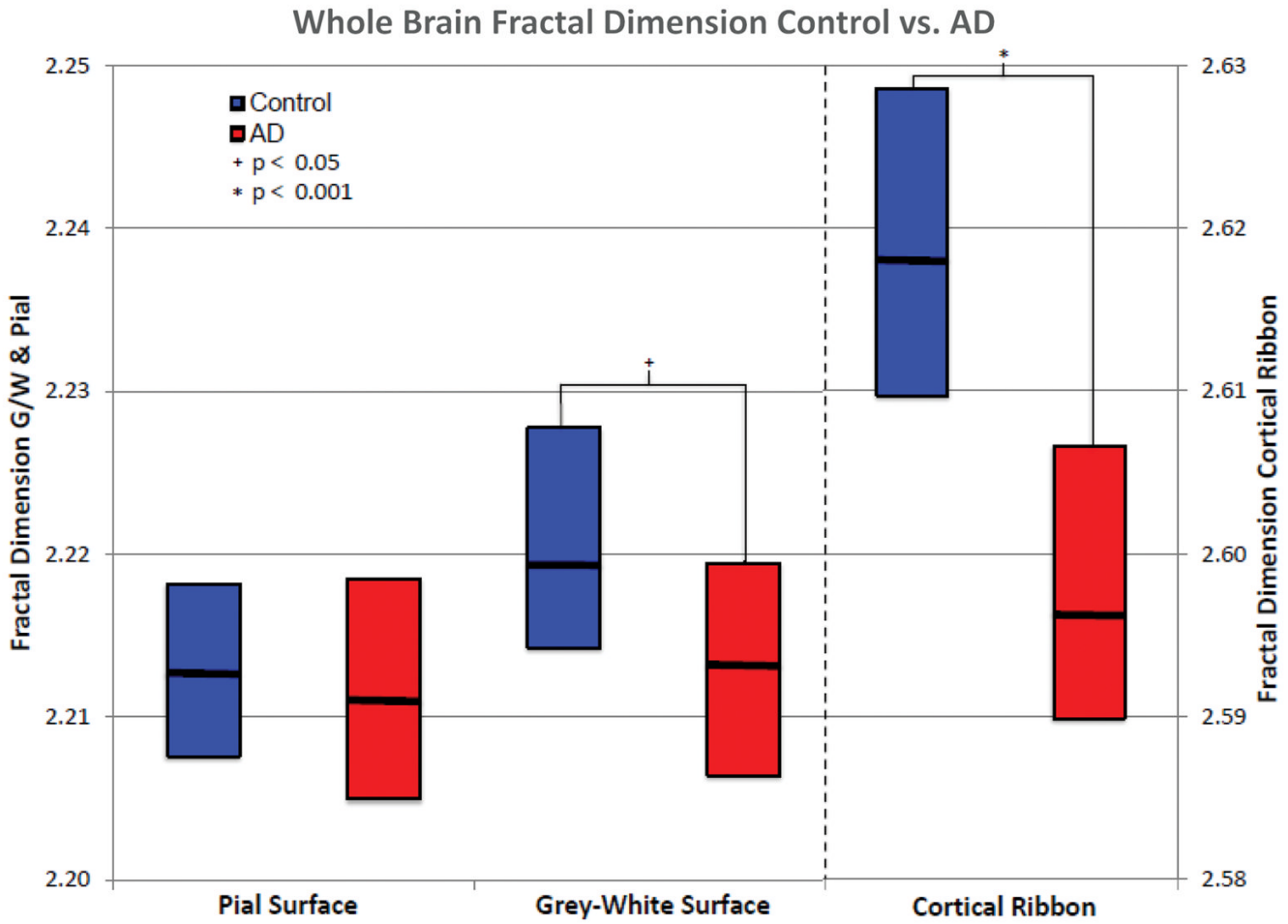

Figure 4. Differences in fractal dimension between groups of normal subjects and patients with mild Alzheimer's Disease (AD) as measured on the pial surface, grey/white surface and the cortical ribbon

The boxes show the median value as the thick black line, and the upper and lower boundaries are the upper and lower quartile, respectively. Normal subjects are in blue, while AD subjects are in red. The pial and grey-white surfaces use the left axis (range 2.20– 2.25). Using the cortical ribbon results in a higher value for the fractal dimension, as shown on the right axis (2.58 – 2.63). Analysis of the cortical ribbon resulted in a much better separation between the two clinical groups.

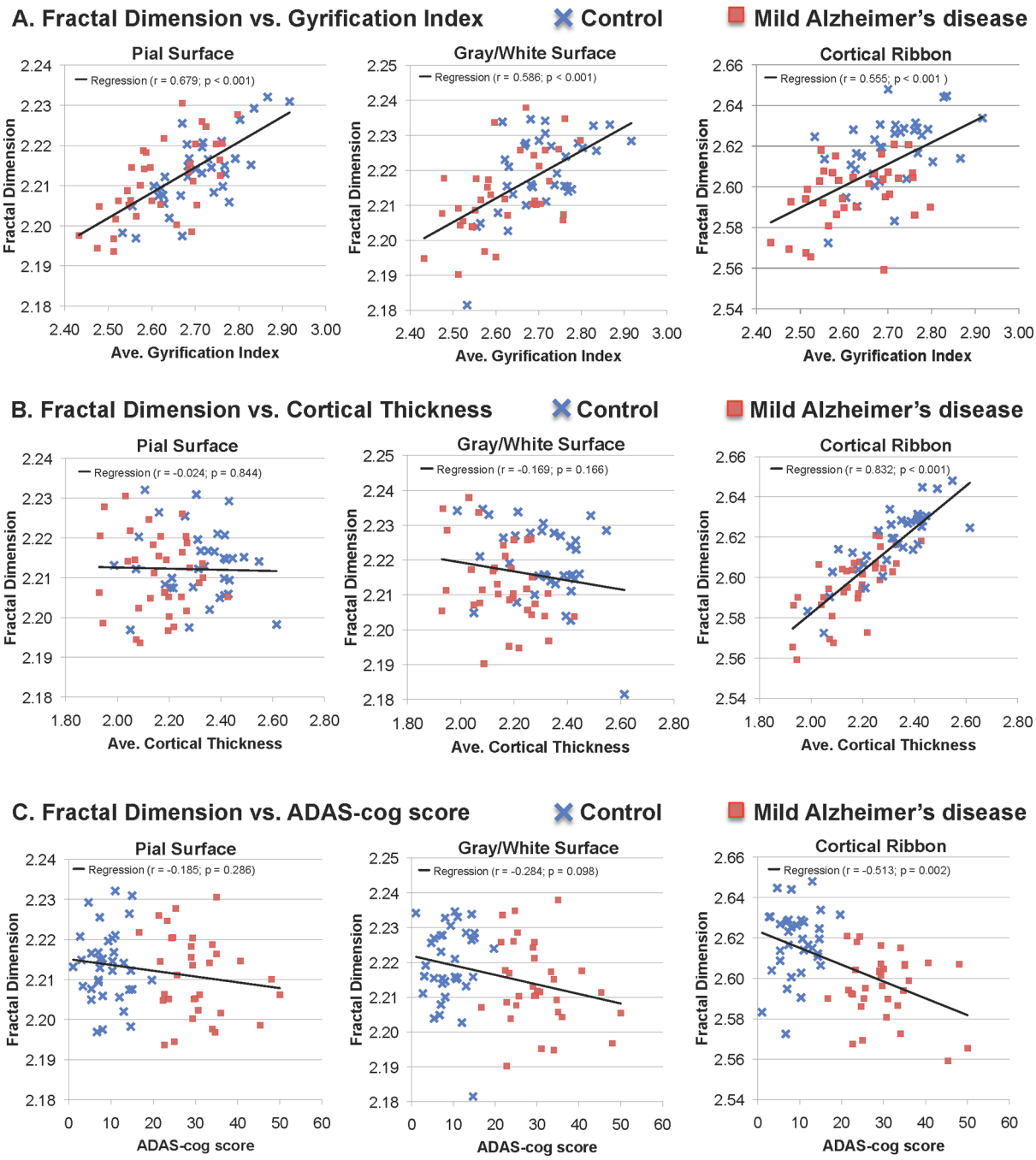

Figure 5. Correlations between the fractal dimension of the three cortical models and gyrification index, cortical thickness, and the ADAS-cog. A. Gyrification Index

All three models have a significant correlation with the gyrification index, with the pial surface having the highest correlation. B. Cortical Thickness: The pial surface is uncorrelated, and the grey/white surface has a trend towards a negative correlation. The ribbon has a strong positive correlation. C. ADAS-cog: Only the cortical ribbon shows a significant correlation with this cognitive neuropsychologic battery of the Alzheimer's Disease Assessment Scale.

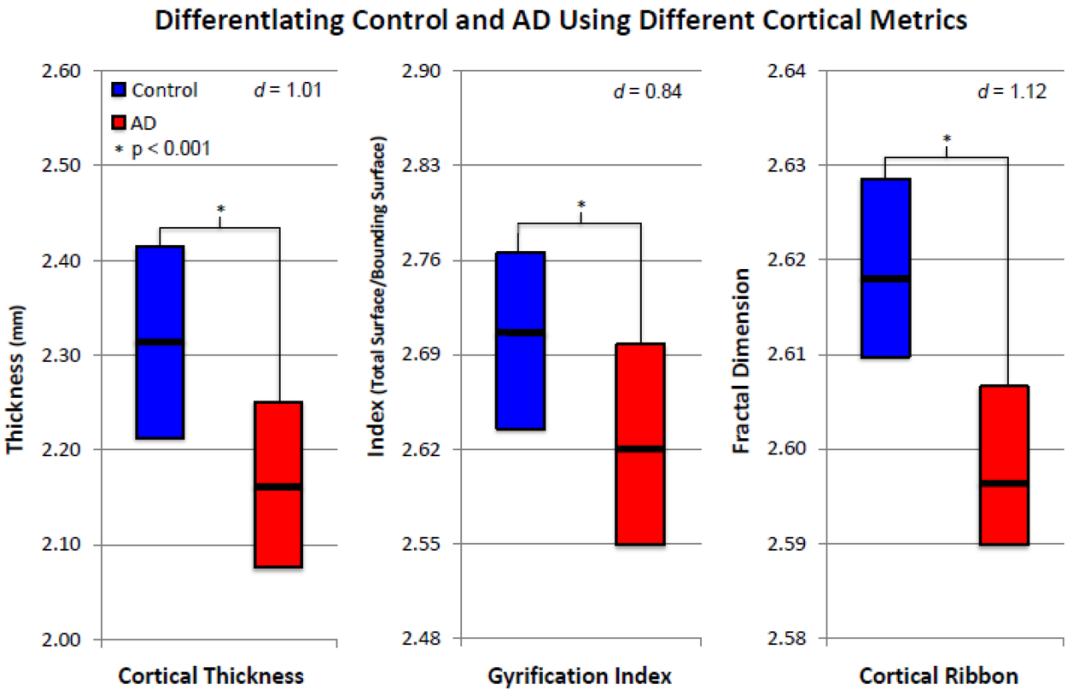

Figure 6. Differences in fractal dimension between groups of normal subjects and patients with mild Alzheimer's Disease (AD) as measured on by cortical thickness, gyrification index, and the cortical ribbon fractal dimension

This figure uses the same conventions as Figure 4. All three measures generated a significant difference between the two groups ($p < 0.001$). The greatest effect size was generated using the cortical ribbon fractal dimension.

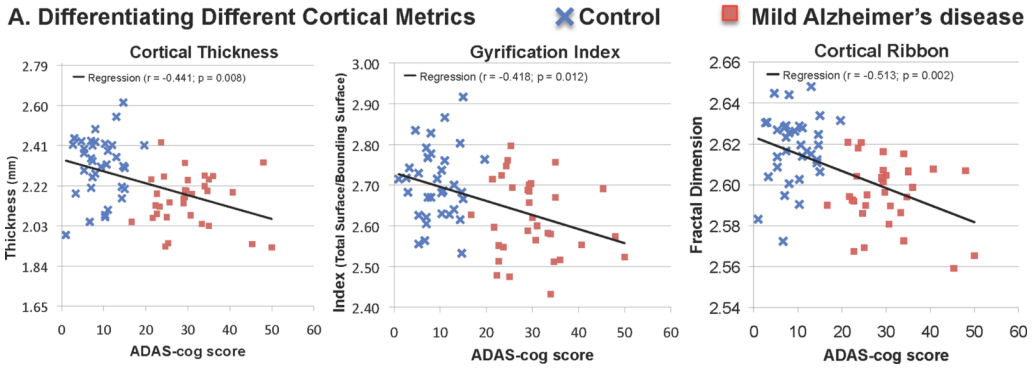

Figure 7. Correlations between the ADAS-cog and cortical thickness, gyrification index, and the cortical ribbon

This figure uses the same conventions as Figure 5. All three cortical metrics have a significant negative correlation with the ADAS-cog scores. The correlation coefficient is of greatest magnitude for the cortical ribbon.

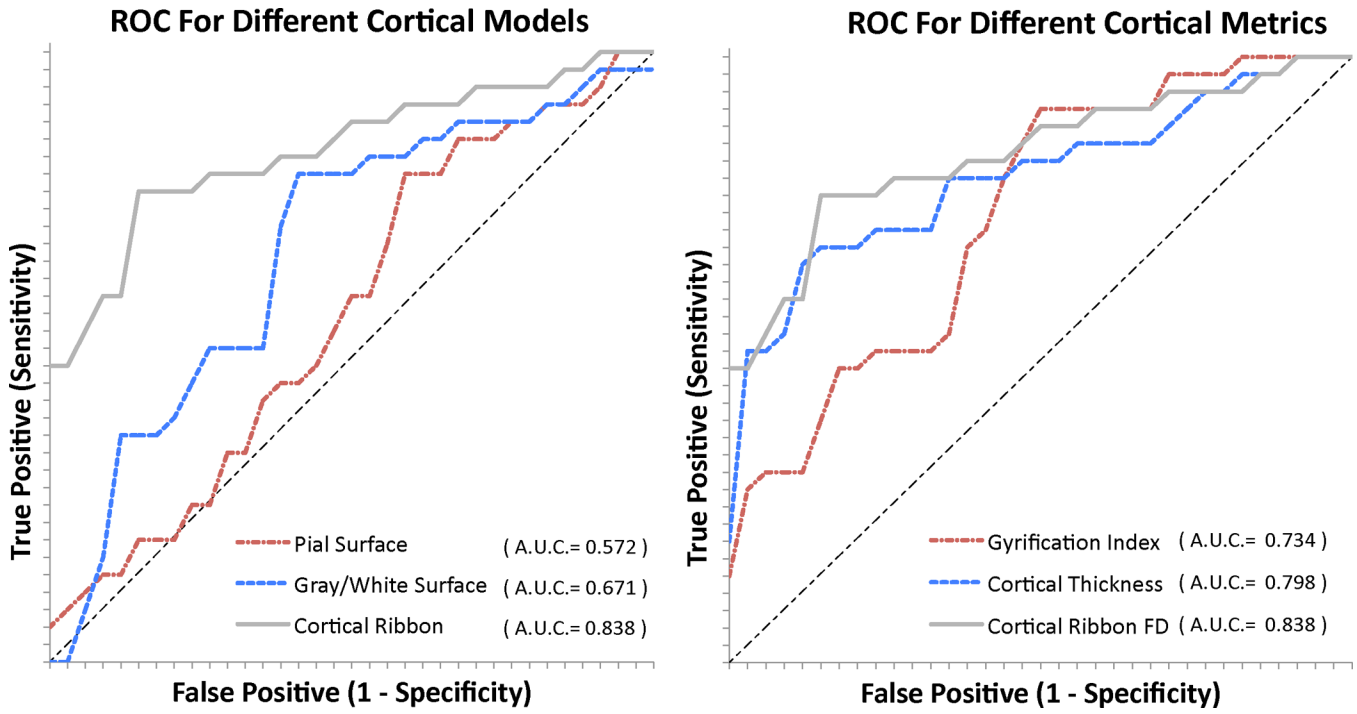

Figure 8. Receiver Operator Curve (ROC) characteristics

ROC curves indicating sensitivity and specificity separating control subject from AD subjects the for each of the measures are shown. Area under the curve values are included in the figure legend. **Left- Cortical Models:** The curves for cortical ribbon f_{3D}, pial surface f_{3D} and grey/white surface f_{3D}. **Right- Cortical Metrics:** The curves for cortical ribbon f_{3D}, cortical thickness, and gyrification index. The cortical ribbon f_{3D} has the highest AUC of all measures used in this paper.

Table 1

Summary of clinical data and computed values

This table shows the values of age, gender, cortical ribbon f_{3D}, pial surface f_{3D}, grey/white surface f_{3D}, average cortical thickness, gyrification index and ADAS-cog score. Two subjects in the mild AD group did not have ADAS-cog scores available at the time of data download. Age and gender are not significantly different between the two groups.

	Age	Sex	Cortical Ribbon f_{3d}	Pial Surface f_{3d}	Grey/White Surface f_{3d}	Cortical Thickness	Gyrification Index	ADAS-cog Score
Control Group	63	M	2.644	2.215	2.233	2.489	2.828	8.0
	66	M	2.611	2.207	2.234	2.215	2.616	14.3
	70	M	2.609	2.208	2.215	2.292	2.626	5.3
	70	M	2.583	2.213	2.234	1.987	2.715	1.0
	70	F	2.631	2.215	2.216	2.445	2.683	3.0
	70	M	2.634	2.231	2.228	2.305	2.917	15.0
	71	F	2.645	2.229	2.226	2.431	2.835	4.7
	71	M	2.590	2.212	2.221	2.072	2.630	10.3
	71	M	2.629	2.215	2.215	2.411	2.767	7.3
	72	F	2.648	2.214	2.228	2.547	2.701	13.0
	72	F	2.631	2.210	2.224	2.412	2.763	19.7
	73	F	2.630	2.221	2.211	2.415	2.718	2.7
	73	M	2.628	2.217	2.228	2.350	2.792	7.0
	73	M	2.606	2.208	2.227	2.205	2.667	15.0
	73	M	2.617	2.206	2.203	2.413	2.628	12.0
	74	M	2.619	2.212	2.216	2.313	2.683	14.7
	74	F	2.604	2.208	2.219	2.183	2.743	3.3
	74	M	2.629	2.215	2.216	2.419	2.737	10.3
	75	M	2.615	2.202	2.213	2.356	2.640	13.0
	76	F	2.626	2.220	2.231	2.311	2.716	9.3
	77	M	2.617	2.213	2.214	2.337	2.769	7.3
	77	M	2.612	2.226	2.226	2.160	2.803	14.3
	78	M	2.627	2.217	2.227	2.375	2.730	5.3
	78	M	2.628	2.221	2.216	2.387	2.760	11.0
	78	F	2.603	2.220	2.235	2.083	2.681	10.3

	Age	Sex	Cortical Ribbon f_{3d}	Pial Surface f_{3d}	Grey/White Surface f_{3d}	Cortical Thickness	Gyrification Index	ADAS-cog Score
	78	M	2.601	2.197	2.210	2.277	2.670	8.0
	78	M	2.625	2.206	2.215	2.428	2.778	8.0
	79	M	2.595	2.210	2.208	2.210	2.605	7.0
	80	M	2.614	2.232	2.233	2.106	2.866	11.0
	80	F	2.619	2.217	2.215	2.321	2.686	10.7
	80	F	2.614	2.205	2.204	2.395	2.555	5.3
	81	F	2.623	2.226	2.228	2.261	2.670	7.3
	81	F	2.628	2.209	2.223	2.433	2.621	7.0
	85	M	2.572	2.197	2.205	2.050	2.564	6.7
	85	M	2.625	2.198	2.181	2.615	2.533	14.7
	59	F	2.621	2.226	2.226	2.251	2.715	21.3
	60	M	2.603	2.209	2.204	2.315	2.544	*
	64	M	2.559	2.199	2.211	1.945	2.691	45.3
	66	M	2.616	2.214	2.210	2.328	2.685	29.3
	68	M	2.607	2.216	2.206	2.251	2.757	35.0
	69	F	2.615	2.219	2.215	2.268	2.580	34.0
	70	F	2.586	2.214	2.217	2.040	2.583	33.3
	71	F	2.599	2.202	2.204	2.266	2.516	36.0
	71	F	2.573	2.198	2.195	2.218	2.432	34.0
Mild AD Group	72	M	2.590	2.228	2.229	1.949	2.797	25.3
	72	F	2.607	2.220	2.221	2.167	2.701	29.3
	72	F	2.606	2.231	2.238	2.030	2.670	35.0
	73	F	2.592	2.206	2.209	2.182	2.552	22.7
	73	F	2.593	2.205	2.218	2.127	2.479	22.3
	74	F	2.621	2.220	2.226	2.265	2.747	24.3
	75	M	2.608	2.215	2.218	2.189	2.554	40.7
	75	M	2.565	2.206	2.205	1.929	2.524	50.0
	76	F	2.590	2.222	2.207	2.049	2.628	16.7
	76	M	2.605	2.213	2.207	2.279	2.758	*
	76	F	2.581	2.202	2.212	2.081	2.565	30.7

Age	Sex	Cortical Ribbon f_{3d}	Pial Surface f_{3d}	Grey/White Surface f_{3d}	Cortical Thickness	Gyrification Index	ADAS-cog Score
77	M	2.596	2.205	2.210	2.197	2.704	29.7
78	M	2.605	2.205	2.212	2.248	2.621	30.0
78	F	2.594	2.214	2.234	2.068	2.597	21.7
78	F	2.618	2.205	2.204	2.426	2.547	23.7
79	F	2.603	2.218	2.213	2.137	2.588	29.0
80	F	2.586	2.221	2.235	1.933	2.761	24.7
80	F	2.602	2.200	2.226	2.200	2.657	29.3
81	M	2.590	2.206	2.195	2.182	2.600	31.0
81	M	2.604	2.215	2.224	2.160	2.689	29.0
84	M	2.595	2.211	2.210	2.141	2.694	25.7
85	M	2.604	2.225	2.217	2.122	2.725	23.3
86	M	2.568	2.194	2.190	2.087	2.513	22.7
86	M	2.569	2.194	2.208	2.072	2.474	25.0
86	F	2.607	2.210	2.197	2.330	2.574	48.0
87	F	2.594	2.197	2.209	2.196	2.512	34.7